35th Annual International Conference of the IEEE EMBS
Osaka, Japan, 3 - 7 July, 2013

An Artificial Neural Network Corrected Blurring Matrix for PET Image Restoration

Jhih-Shian Lee[1], and Jyh-Cheng Chen[1*]

Abstract—**Restoration allows recovery of an image that has been blurred by using a priori knowledge of the blurring matrix and statistics of the noise. Therefore, it is important to obtain an accurate blurring matrix before restoring an image. The purpose of this study was to correct the blurring matrix using an artificial neural network (ANN). A Mini Deluxe Phantom™ was used to acquire images from microPET® R4 and a high-resolution optical scanner for ANN training. The images acquired using the two devices served as the inputs and outputs of a single-layer adaptive linear neuron network (ADALINE) for correcting the blurring matrix, which was further used for PET image restoration using Lucy-Richardson algorithm. The normalized root mean square error coefficient of variation and contrast recovery of the resorted images using the ANN corrected blurring matrix (BM_{ANN}) performed better than those without using the ANN. The spatial resolution (FWHM) of the restored image is better and more uniformly distributed than the original one. The CR is also better. The results suggested that blurring matrix can be improved by the ANN.**

I. Introduction

Positron emission tomography (PET) images were blurred due to the positron range, non-colinearity, depth-of-interaction, and other factors. Those physical effects result in partial volume effect (PVE) and degrade the quality of PET images. Low image quality may lead to misdiagnosis. Furthermore, PVE needs to be corrected when calculating the standardized uptake value (SUV), delineating the tumor volume, or performing quantitative small animal studies [1, 2]. PVE is an important issue in case of low spatial resolutions compared to that of high resolutions. Therefore, image resolution improvement is important to reduce PVE.

The blurred PET image can also be described by a shift-variant point spread function (PSF) [3, 4]. PSF means that after data acquisitions, a point spreads into a blurring function. The PSF of PET is known as spatially shift-variant [3, 4]. The response of the PET system to a point source is different when the point source is placed in different places. Image restoration attempts to estimate an image that has been blurred by using a priori knowledge of the blurring matrix (BM) and statistics of the noise. Therefore many image restoration algorithms such as the Lucy-Richardson algorithm (L-R) [5, 6] and iterative thresholding algorithm [7, 8], estimate blurring images as the linear combination of the BM and estimated sharp image and can be written as:

$$\hat{\mathbf{y}} = \mathbf{H}\hat{\mathbf{x}}, \tag{1}$$

where **H** is the blurring matrix (BM).

Thus many researchers tried to acquire the BM before obtaining the estimate of the true object [9-12]. A well-modeled BM can describe the relationship between the object and PET image and can be used to restore the PET image with better quality. Therefore the purpose of this study was to use ANN to correct the errors of a BM, which is approximated by a piecewise-linear interpolation for image restoration and further improve the quality of resorted images. The Lucy-Richardson (L-R) algorithm [5, 6] is also used to restore PET images with BM_{ANN}. We also compared the image quality of the restored image using BM_{ANN} with the BM which is approximated by piecewise-linear interpolation (BM_{Linear}).

II. Materials and Methods

A. Lucy-Richardson algorithm

The L-R algorithm is a statistic iterative restoration method for recovering an image that has been blurred by a known BM [5, 6]. The L-R algorithm is the maximum-likelihood solution for Poisson statistical data and is defined in the following equation:

$$\hat{\mathbf{x}}_{n+1} = \hat{\mathbf{x}}_n \left[\mathbf{H}^T \left[\frac{\mathbf{y}}{\mathbf{H}\,\hat{\mathbf{x}}_n} \right] \right], \tag{2}$$

where $\hat{\mathbf{x}}$ is the input of the system, the estimated sharp image, **y** is a blurred image that is blurred by a shift-variant BM, **H**. In this equation, each vector operates point-by-point with each other and n indicates the results of the n^{th} iteration. We chose L-R to restore images with BM_{ANN} and BM_{Linear}.

B. ANN for correcting system matrix

In order to correct the errors of an approximated BM, a single-layer adaptive linear neuron network (ADALINE) [13, 14] with a bias vector and a positive constraint was used. As the single-layer architecture and linear output activation function, F(x) = x, were selected, the output of neuron can be written similar to (1) as follows:

$$\mathbf{y}^k = \mathbf{W}^k\mathbf{x} - \mathbf{b}^k, \tag{3}$$

*: corresponding author
J.C. Chen is with Department of Biomedical Imaging & Radiological Sciences, National Yang-Ming University, No. 155, Sec. 2, Linong Street, Taipei, 112 Taiwan (corresponding author to provide phone: +886-2-2827-7282; fax: +886-2-2820-1095; e-mail: jcchen@ym.edu.tw).
J.S. Lee is with Department of Biomedical Imaging & Radiological Sciences, National Yang-Ming University, No. 155, Sec. 2, Linong Street, Taipei, 112 Taiwan (e-mail: jhihshianlee@gmail.com).

where $\mathbf{y}^k$ is the neuron output, $\mathbf{x}$ is the neuron input, $\mathbf{W}^k$ is the weight matrix and $\mathbf{b}^k$ is the bias. In this study, PET images are treated as desired outputs, and neuron inputs, the sharp images, were generated by a high-resolution optical scanner. The single neural network, ADALINE, is simple with fast training speed. Moreover, the equation of ADALINE is identical to the relationship between the PET image and the sharp image as shown in Eq.(1). This means that the weight matrix $\mathbf{W}$ is a BM.

The ADALINE uses the simple gradient descent algorithm to minimize the square error for ANN training with 10000 iterations. Therefore, the generalized delta rule learning algorithm (GDR) was used to minimize the error between the network and desired output by supervised learning[13, 14], which can be described as follows:

$$\Delta \mathbf{W} = L\boldsymbol{\delta}^k \mathbf{x} \quad , \quad \mathbf{W}^{k+1} = \mathbf{W}^k + \Delta \mathbf{W}^k , \tag{4}$$

$$\Delta \mathbf{b} = L\boldsymbol{\delta}^k \mathbf{x} , \quad \mathbf{b}^{k+1} = \mathbf{b}^k + \Delta \mathbf{b}^k , \tag{5}$$

where $\Delta\mathbf{W}$ is the matrix for updating $\mathbf{W}$, $\Delta\mathbf{b}$ is the vector for updating $\mathbf{b}$, L is the learning rate ,and $\mathbf{x}$ is the neuron input. In this equation, $\boldsymbol{\delta}^k$ is defined as follows:

$$\boldsymbol{\delta}^k = \mathbf{d} - \mathbf{y}^k , \tag{6}$$

where $\mathbf{d}$ is the desired output and $\mathbf{y}$ is the neuron output. For increasing rates of convergence, we also used the momentum learning algorithm [15]. The matrix for updating W is described as follows:

$$\Delta \mathbf{W}^k = rL\,\boldsymbol{\delta}^k \mathbf{x} + (1-r)\Delta \mathbf{W}^{k-1} , \tag{7}$$

where r is the momentum term. The learning rate of GDR is a scalar.

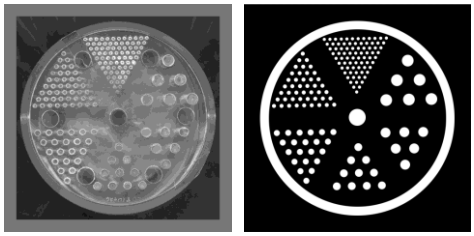

(A) (B)

Figure 1. (A) Mini Deluxe cold-rod phantom (B) Digital phantom for ANN inputs. The binary sharp images were segmented from the image scanned by a high resolution optical scanner.

C. Network training using a physical phantom

The cold-spot Mini Deluxe Phantom™ was used to acquire PET images and optical scanner images for ANN training. Here is the specification of this phantom: rod diameters: 1.2, 1.6, 2.4, 3.2, 4.0 and 4.8 mm; height of rods: 3.4 cm; insert diameter: 7.5 cm; cylinder outer diameter: 8.3 cm; cylinder inner diameter: 7.6 cm; cylinder inside height: 3.8 cm (Fig. 1). There are 33 input and desired output pairs with different orientations (Fig. 2). The sharp input images were acquired using the Epson perfection 1240U optical scanner with pixel size of 0.01 mm. Then, the scanned image was segmented manually to form a binary sharp image (Fig. 1). After the radioisotope, ^{18}F solution, was filled into the physical phantom, the desired outputs, PET images, were obtained from the cold spot Mini Deluxe Phantom with the corresponding orientations with respect to the microPET® R4. All PET images were acquired at rest for 3600s. After emission scanning, a 30 min transmission scan was taken with the ^{68}Ge or ^{57}Co transmission source. After segmented the transmission image into air, water and Lucite, the segmented transmission image was used for attenuation and single-scatter simulation scatter corrections [16]. After Fourier rebinning, the PET images were reconstructed using the filtered backprojection method. The pixel size of the reconstructed images is 0.423 × 0.423 × 1.121 mm. Correction for random events, radioactive decay, attenuation, scatter, and dead time was performed during reconstruction. Then we performed the rigid body transformation and re-sampled pixel size of the scanned image to align manually the input–output training pairs using the commercial software PMOD (PMOD Technologies, Zurich, Switzerland). Before ANN training, the total counts of input images were normalized to be the same as the corresponding desired output, the PET image.

We used a multi-line hot-in-water phantom to obtain an initial guess of the BM for ANN (Fig. 3). First, we fitted each PSF in the PET image of the multi-line hot-in-water phantom using the asymmetrical Gaussian model. We then interpolated the variances in the adjacent regions using linear interpolation [11, 12]. Then the BM_{Linear} was calculated using the interpolated variances.

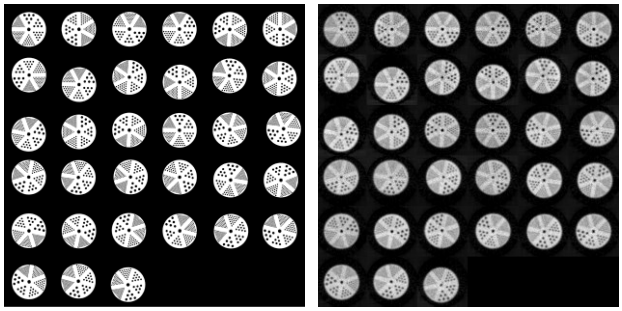

(A) (B)

Figure 2. Thirty three digital training sets with different orientations

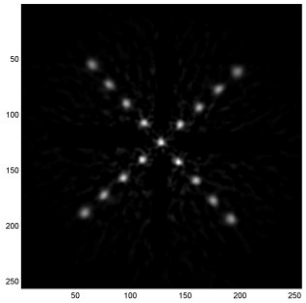

Fig. 3. (A) The PET image of the multi-line hot-in-water phantom

D. Evaluation method

The normalized root mean square error (NRMSE) is defined in Eq.(8).

$$\text{NRMSE} = \sqrt{\frac{\sum_{i=1}^{N} [\mathbf{y}_{\text{Estimated}}(i) - \mathbf{x}(i)]^2}{\sum_{i=1}^{N} [\mathbf{x}(i)]^2}}, \quad (8)$$

where $\mathbf{x}$ is the sharp image obtained by an optical scanner, $\mathbf{y}_{\text{Estimated}}$ is the restored image. The NRMSE was used to evaluate the difference between the data and their references.

The coefficient of variation (CV) can be used to evaluate the uniformity of the image. CV can be defined in the following equation:

$$\text{CV} = \frac{\text{std}(\mathbf{r}_1)}{\text{mean}(\mathbf{r}_1)}, \quad (9)$$

where $\mathbf{r}_1$ belongs to a uniform area of the image. We selected regions of interest (ROIs) in the uniform area of the images of the Mini Deluxe Phantom™ (one was inserted with cold spots and the other was inserted with hot spots) to evaluate our method (Fig. 4 B).

Contrast recovery (CR) represents the contrast between the signal and background and can be defined as follows:

$$\text{CR} = 1 - \frac{\text{mean}(\mathbf{r}_2)}{\text{mean}(\mathbf{r}_1)}, \quad (10)$$

where $\mathbf{r}_1$ belongs to the target of the image (Fig. 4 C) and $\mathbf{r}_2$ belongs to a background area (Fig. 4 B).

The full-width-at-half-maximum (FWHM) is a figure of merit to evaluate the spatial resolution. Narrow FWHM indicates better resolution, while wider FWHM indicates worse resolution. We fitted each PSF in the images of the multi-line hot-in-water phantom using an asymmetrical Gaussian model. The FWHM is defined as follows:

$$\text{FWHM} = 2\sqrt{2\ln(2)}\,\sigma_{average}, \quad (11)$$

where $\sigma_{average}$ is the mean value of σ in different directions.

(A) (B) (C)

Figure 4. (A) PET image of the Mini-Deluxe phantom, (B) uniform and background area of the image, and (C) target area of the image.

TABLE I. NRMSEs, CVs, AND CRs

	NRMSE	CV	CR
Original	0.34	0.08	0.66
BM_{Linear}	0.32	0.13	0.84
BM_{ANN}	0.31	0.11	0.88

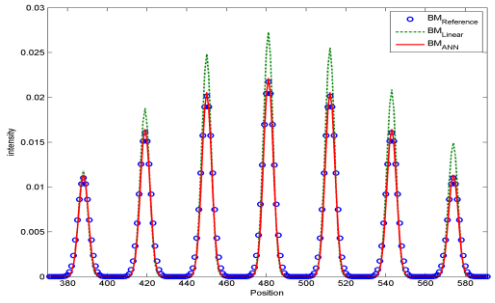

Figure 5. The profiles of a PSF in $BM_{Reference}$ (original measured PSF), BM_{Linear} (initial) and BM_{ANN} (result).

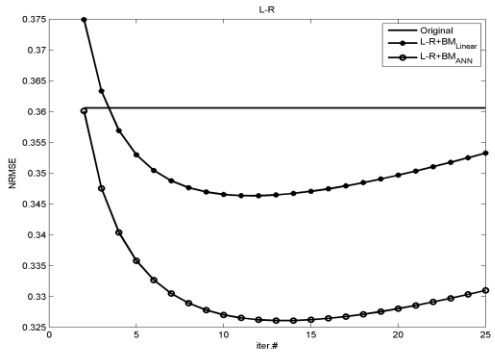

Figure 6. NRMSE of different iteration numbers.

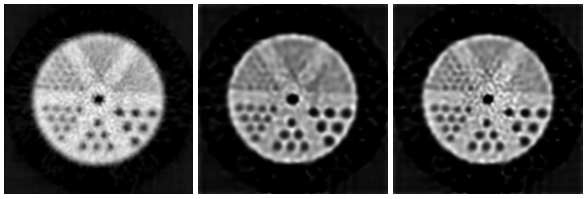

(A) (B) (C)

Figure 7. (A) Original image (B) L-R algorithm with BM_{Linear} (C) L-R algorithm with BM_{ANN}

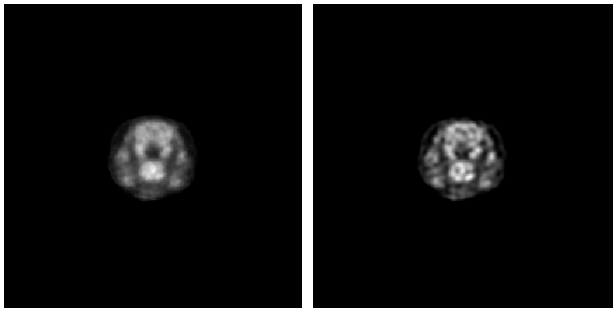

(A) (B)

Figure 8. (A) Original rat brain image (B) After restoration using L-R algorithm with BM_{ANN}

TABLE II. FWHMs (MM) MEASURED FROM THE HOT-IN-WATER PHANTOM

	-3 cm	-2 cm	-1 cm	0 cm	1 cm	2 cm	3 cm
Original	3.05	2.58	2.27	2.12	2.32	2.48	2.91
BM_{Linear}	2.46	2.19	1.74	1.70	1.83	2.11	2.40
BM_{ANN}	2.28	1.76	1.54	1.51	1.62	1.79	2.30

III. Results

To evaluate the ability of ANN for correcting BM, we used a measured PSF to compare with corrected PSF. The location of the measured PSF was different from the locations of all the PSFs measured by the multi-line hot-in-water phantom. The corresponding profiles of the PSF are showed in Fig. 5. Figure 6 shows the NRMSE of different iteration numbers. Table I shows the RMSEs, CVs, and CRs of 10 iterations. Table II shows FWHMs measured from the hot-in-water phantom. A phantom case with 10 iterations was showed in Fig. 7. A rat brain case with 10 iterations was showed in Fig. 8.

IV. Discussion

The most technical limitation of PET is low spatial resolution. Several groups investigate methods to restore PET image. Image restoration is to estimate original object given knowledge of blurred image, BM, and the statistics of noise. In this study, we used ANN to correct BM for better results of image restoration. In this study, we do not use the optimal images as output and the PET images as input of the ANN because the initial guess of the inverse of BM is hard to estimate. If the initial guess is far away from exact solution, then more training sets are needed to estimate the exact solution. Figure 4 show profiles of a measured PSF, the initial PSF, and the ANN corrected PSF. The results show that after ANN training, the profile of PSF would move toward the reference from the initial guess. The NRMSE, CV, CR of resorted images using ANN corrected blurring matrix is better than those without ANN (Table I). The resolution (FWHM) of the restored image is better and more uniformly distributed than the original one (Table II). The ANN approach can learn PSFs that were not included or were not corrected in the BM from real data. The computing time when applying ANN to correct BM of an image with a size of $256 \times 256 \times 63$ is about one day. However the corrected BM is reusable if the imaging system is not changed. Furthermore the advantage of the ANN approach is that the ANN method can directly learn the PSF from real data, which might not be described correctly using interpolated BM_{Linear} from measured PSFs from a multi-line-hot-in water phantom. However, errors occurred by the manual registration for input and output training sets. Although the commercial software PMOD was used, the contours of PET images were spread into an area because of the PVE. That may greatly degrade the efficiency of ANN corrected BM. Therefore, this ANN approach is suitable to be applied in a PET/CT scanner or PET/MRI scanner which does not need manual registration. The CT and MRI can also provide high-resolution images for ANN input. Thus, the image quality of the PET can be further improved by using the multimodality scanners.

V. Conclusion

PET images are blurred due to the shift variant PSF. According the result, the resolution of the restored image using L-R algorithm and BM_{ANN} is more uniform and sharp than the original image. The results of this study suggest that the BM can be updated toward ideal BM using ANN for image restoration. Therefore, the ANN approach can be used to improve image restoration of PET.

Acknowledgment

The authors would like to thank the National Science Council of the Republic of China, Taiwan, for financially supporting this research under Contract No. NSC 101-2627-E-010-001

References

[1] M. Soret, *et al.*, "Partial-volume effect in PET tumor imaging," *Journal of Nuclear Medicine,* vol. 48, p. 932, 2007.

[2] K. H. Su, *et al.*, "Image segmentation and activity estimation for microPET 11C-raclopride images using an expectation-maximum algorithm with a mixture of Poisson distributions," *Computerized Medical Imaging and Graphics,* vol. 35, pp. 417–426, 2011.

[3] B. Karuta and R. Lecomte, "Effect of detector weighting functions on the point spread function of high-resolution PET tomographs: a simulation study," *IEEE Transactions on Medical Imaging,* vol. 11, pp. 379-385, 1992.

[4] D. Schmitt, *et al.*, "Fast point spread function computation from aperture functions in high-resolution positron emission tomography," *IEEE Transactions on Medical Imaging,* vol. 7, pp. 2-12, 1988.

[5] L. Lucy, "An iterative technique for the rectification of observed distributions," *The astronomical journal,* vol. 79, p. 745, 1974.

[6] W. H. Richardson, "Bayesian-based iterative method of image restoration," *JOSA,* vol. 62, pp. 55-59, 1972.

[7] C. Vonesch and M. Unser, "A fast iterative thresholding algorithm for wavelet-regularized deconvolution," in *Proc. SPIE 6701, Wavelets XII, 67010D*, 2007, pp. 183-202.

[8] M. A. T. Figueiredo and R. D. Nowak, "An EM algorithm for wavelet-based image restoration," *IEEE Transactions on Image Processing,* vol. 12, pp. 906-916, 2003.

[9] V. Y. Panin, *et al.*, "Fully 3-D PET reconstruction with system matrix derived from point source measurements," *IEEE Transactions on Medical Imaging,* vol. 25, pp. 907-921, 2006.

[10] K. Knesaurek and J. Machac, "Improving 3D PET imaging by restoration: a phantom study," *Computerized Medical Imaging and Graphics,* vol. 29, pp. 15-19, 2005.

[11] J. G. Nagy and D. P. O'leary, "Fast iterative image restoration with a spatially-varying PSF," in *Proc. SPIE 3162, Advanced Signal Processing: Algorithms, Architectures, and Implementations VII*, 1997, pp. 388-401.

[12] J. G. Nagy and D. P. O'Leary, "Restoring images degraded by spatially variant blur," *SIAM Journal on Scientific Computing,* vol. 19, pp. 1063-1082, 1998.

[13] K. H. Su, *et al.*, "A Novel Method to Improve Image Quality for 2-D Small Animal PET Reconstruction by Correcting a Monte Carlo-Simulated System Matrix Using an Artificial Neural Network," *IEEE Transactions on Nuclear Science,* vol. 56, pp. 704-714, 2009.

[14] M. T. Hagan, *et al.*, *Neural network design*: PWS Boston, MA, 1996.

[15] R. A. Jacobs, "Increased rates of convergence through learning rate adaptation," *Neural networks,* vol. 1, pp. 295-307, 1988.

[16] C. Watson, "New, faster, image-based scatter correction for 3D PET," *IEEE Transactions on Nuclear Science,* vol. 47, pp. 1587-1594, 2000.